Hand-eye Calibration with a Depth Camera: 2D or 3D?

Svenja Kahn[1], Dominik Haumann[2] and Volker Willert[2]
[1]*Fraunhofer IGD, Darmstadt, Germany*
[2]*Control Theory and Robotics Lab, TU Darmstadt, Darmstadt, Germany*

Keywords: Hand-eye Calibration, Depth Cameras, Pose Estimation, Image based Calibration, Geometric Alignment, 3D Measurements, Iterative Closest Point Algorithm, Comparative Evaluation.

Abstract: Real time 3D imaging applications such as on the fly 3D inspection or 3D reconstruction can be created by rigidly coupling a depth camera with an articulated measurement arm or a robot. For such applications, the ”hand-eye transformation” between the depth camera and the measurement arm needs to be known. For depth cameras, the hand-eye transformation can either be estimated using 2D images or the 3D measurements captured by the depth camera. This paper investigates the comparison between 2D image based and 3D measurement based hand-eye-calibration. First, two hand-eye calibration approaches are introduced which differ in the way the camera pose is estimated (either with 2D or with 3D data). The main problem in view of the evaluation is, that the ground truth hand-eye transformation is not available and thus a direct evaluation of the accuracy is not possible. Therefore, we introduce quantitative 2D and 3D error measures that allow for an implicit evaluation of the accuracy of the calibration without explicitly knowing the real ground truth transformation. In view of 3D precision, the 3D calibration approach provides more accurate results on average but requires more manual preparation and much more computation time than the 2D approach.

1 INTRODUCTION

Depth cameras capture dense 3D point clouds in real time. Tasks such as 3D difference detection, bin-picking or simultaneous localization and mapping can be addressed by rigidly coupling a depth camera with an articulated measurement arm or with a robot (Fuchs, 2012)(Kahn et al., 2013). To transform the 3D measurements of the depth camera into the coordinate system of the articulated arm, the relative transformation between the depth camera and the measurement arm needs to be known. This transformation is called ”hand-eye transformation”.

For 2D color cameras, estimating the hand-eye calibration between the 2D camera and a robot or a coordinate measuring machine such as a measurement arm is a well researched task (Tsai and Lenz, 1988)(Strobl and Hirzinger, 2006). Recently, the technological advances of real-time depth imaging brought up the question how to estimate the hand-eye transformation for 3D depth cameras. As most depth cameras also output a 2D intensity image in addition to the depth measurements, an obvious solution is to use the same algorithms for depth cameras as for 2D color cameras. For instance, Reinbacher employed such an image based approach for the hand-eye calibration between a depth camera and a robot (Reinbacher et al., 2012). Kahn described an image based hand-eye calibration between a depth camera and an articulated measurement arm (Kahn and Kuijper, 2012). In contrast to these 2D image based hand-eye calibration procedures, Kim used the 3D measurement at the center of a marker for the hand-eye calibration (Kim and Ha, 2013). Fuchs proposed a solution which uses depth measurements instead of 2D images (Fuchs, 2012). This approach employs a calibration plane with known position and orientation. The hand-eye calibration is estimated by solving a least squares curve fitting problem of the measured depth values with the calibration plane.

While both 2D and 3D data based approaches have been proposed, little is known about the accuracy and the suitability of these approaches for the hand-eye calibration with a depth camera. The accuracy of the hand-eye transformation is either not evaluated at all (Reinbacher et al., 2012)(Kahn and Kuijper, 2012) or just for specific calibration procedures (Fuchs, 2012). This complicates the decision whether to estimate the hand-eye transformation with a 2D or with a 3D data based approach. It is unknown whether 2D data based approaches have major advantages compared to 3D data based approaches (or vice

Kahn S., Haumann D. and Willert V..
Hand-eye Calibration with a Depth Camera: 2D or 3D?.
DOI: 10.5220/0004668604810489
In *Proceedings of the 9th International Conference on Computer Vision Theory and Applications* (VISAPP-2014), pages 481-489
ISBN: 978-989-758-009-3

versa), or whether both kinds of approaches can provide comparable results.

This paper contributes to this unsolved research question with three main contributions. First, we propose a 3D measurement based hand-eye calibration using the same transformation estimation principle as a previously published 2D image based hand-eye calibration procedure (Kahn and Kuijper, 2012). The difference between both approaches is the way the position and orientation of the depth camera is estimated: either by analyzing the captured 2D image, or by geometrically aligning the 3D measurements with a 3D model of the calibration object. This deliberate algorithmic design choice makes it possible to directly compare the 2D image based and the 3D data based approach. Second, we propose to use both a 2D data based and a 3D data based evaluation criterion. The reason for this is that a calibration, which is consistent with the 2D data, is not necessarily accurate in the 3D space (and vice versa). Third, we provide a comparative quantitative evaluation of both the 2D and the 3D data based hand-eye calibration, both for a structured light depth camera (Kinect) and a time-of-flight depth camera (SwissRanger 4000).

In this paper, we estimate the hand-eye transformations between a Faro Platinum measurement arm and depth cameras rigidly coupled to this arm (see Figure 1). The arm has a measurement range of 3.7 meters. It outputs the position and orientation of its point tip with a precision of 0.073mm. The approaches described in this paper are not only applicable for measurement arms, but also for other hand-eye calibrations, for example between a robot and a depth camera. As a preparation step, the intrinsic calibration parameters (focal length, principal point and the distortion parameters) of the depth cameras were calculated with the GML camera calibration toolbox.

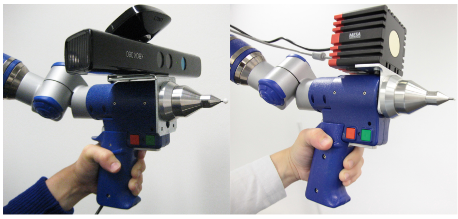

(a) Kinect (b) SwissRanger 4000

Figure 1: Depth cameras rigidly coupled with a Faro measurement arm.

The remainder of this paper is structured as follows. First, Section 2 and Section 3 describe the 2D image based and the 3D measurement based hand-eye calibration approaches. Then, Section 4 introduces the error metrics for evaluating the hand-eye calibrations. The two hand-eye calibration approaches are evaluated quantitatively in Section 5, both for a Kinect and a SwissRanger 4000 depth camera. Finally, conclusions are drawn in Section 6 and possible adaptations for future work are proposed.

2 2D IMAGE BASED HAND-EYE CALIBRATION

For a depth camera, the hand-eye transformation can be estimated in a similar way as for a 2D color camera. In this paper, we use the image based hand-eye calibration described by Kahn for a depth camera and an articulated measurement arm (Kahn and Kuijper, 2012). The image based hand-eye calibration is summarized in this section.

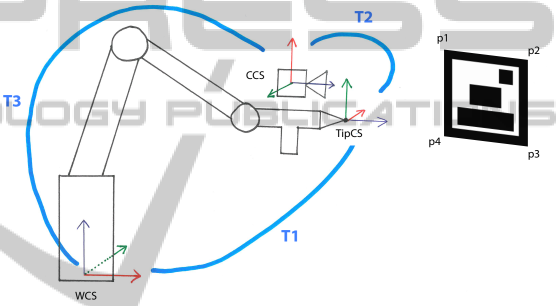

Figure 2: Image based Hand-Eye Calibration (Kahn and Kuijper, 2012).

Figure 2 visualizes a sketch of the measurement arm, the depth camera and an image marker which is used to calculate the hand-eye calibration with this image based approach. We define the world coordinate system (WCS) as the coordinate system of the measurement arm. The measurement arm outputs the transformation T1, which is the relative transformation between the measurement tip's coordinate system (TipCS) and the coordinate system of the base of the measurement arm (WCS). The transformation T2 is the hand-eye transformation between the coordinate system of the depth camera (CCS) and TipCS. T3 is the camera pose relative to the world coordinate system. Once the hand-eye transformation is known, the camera pose can be calculated from the pose of the measurement arm and the hand-eye transformation with

$$\begin{aligned} R_3 &= R_2 \cdot R_1, \\ t_3 &= R_2 \cdot t_1 + t_2. \end{aligned} \tag{1}$$

In the notation of Equation (1), each transformation Ti is split up into its rotational and translational component (R_i and t_i). The equation used to calculate the hand-eye calibration $T2_j$ is specified in Equation (2) (it can easily be inferred from Equation (1)). The hand-eye transformation is calculated from n pose pairs ($T1_j$, $T3_j$) with $1 \leq j \leq n$. Each such pair contains a pose of the measurement arm's point tip and a depth camera pose, both relative to the world coordinate system. Theoretically, the hand-eye calibration could be approximated by a single pose pair. However, to improve the accuracy, many pose pairs are captured and $T2_j$ is calculated for each pose pair. Then, each rotational and translational parameter of the final hand-eye calibration is the median of this parameter in all collected $T2_j$ transformations. The median is used to calculate the final hand-eye transformation because it is more robust against outliers than the mean values.

$$\begin{aligned} R_2 &= R_3 \cdot {R_1}^{-1} \\ t_2 &= t_3 - R_2 \cdot t_1 \end{aligned} \tag{2}$$

Image based Depth Camera Pose Estimation. The pose of a camera can be calculated from a set of 2D-3D correspondences. Each such 2D-3D correspondence stores the position of a 3D point in the world coordinate system and its 2D projection onto the image coordinate system of the camera. We use a 2D calibration pattern to obtain such 2D-3D correspondences. Here, the 2D calibration pattern is an image marker which can also be robustly detected with depth cameras which have a lower resolution than standard color cameras. This 2D calibration pattern is attached to a planar surface in the working range of the measurement arm and the 3D positions of its four corners ($p1$, ..., $p4$) are measured with the point tip of the measurement arm. The measured 3D coordinates are in the base coordinate system of the measurement arm (which is the world coordinate system).

Then, the calibration pattern is detected in the 2D image captured by the depth camera. Time-of-flight depth cameras directly measure an intensity (grey) value for each captured pixel, which can be used to detect the 2D pattern. In contrast to time-of-flight cameras, per default the depth camera of the Kinect only outputs a depth value per pixel and no color or intensity information. However, the Kinect depth camera can be switched from depth to infrared acquisition mode. Thus, it is possible to detect the calibration pattern in the infrared image of the depth camera and to estimate the pose of the Kinect depth camera based on the detected 2D pattern.

The four 2D-3D correspondences (2D point in the image and the 3D coordinate of the detected 2D point in the WCS) as well as the intrinsic parameters of the depth camera and an image of the marker are the input for the camera pose estimation. The depth camera's pose $T3_j$ is estimated with direct linear transformation (DLT) and a subsequent nonlinear least squares optimization.

3 GEOMETRIC 3D HAND-EYE CALIBRATION

The principle of the geometric hand-eye calibration is similar as the image based approach sketched in Figure 2. Just as for the image based approach, the transformation T1 is output by the measurement arm and T3 (the pose of the depth camera in the world coordinate system) is estimated for each single frame. Then, the hand-eye calibration T2 is estimated from T1 and T3 as specified by Equation (2). The difference between both approaches is that for the geometric approach, the pose of the depth camera (T3) is not calculated with image based camera tracking. Instead, it is estimated by geometrically aligning 3D measurements on the surface of the real calibration object (captured with a depth camera) with a virtual 3D model of the calibration object. Therefore, the geometric hand-eye calibration described in this section requires a 3D model of the calibration object.

Calibration Object and 3D Model. Figure 3 shows a calibration object and a virtual 3D model of the calibration object. The calibration object was designed such that it accounts for the specific 3D measurement properties of depth cameras (Willert et al., 2012). The measurement accuracy of depth cameras depends strongly on the surface of the captured object. For instance, at jump edges or on object surfaces which absorb most of the light emitted by time-of-flight depth cameras, the measurement accuracy of these depth cameras is poor (Piatti, 2011)(Stoyanov et al., 2012). Therefore, the curved surface of the calibration object was designed such that no jumping edges occur on its front surface when the depth camera is moved in front of it. Furthermore, it consists of a material which diffusely reflects most of the light emitted by time-of-flight depth cameras and which thus supports the precision of the depth measurements. Additionally, the shape of the calibration object is designed in such a way that only one unique 3D alignment exists (neither symmetries nor periodicities).

Alignment of the Virtual 3D Model with the Real Calibration Object. Before the camera pose can be estimated with geometric alignment, as a preparation step, the virtual 3D model needs to be transformed

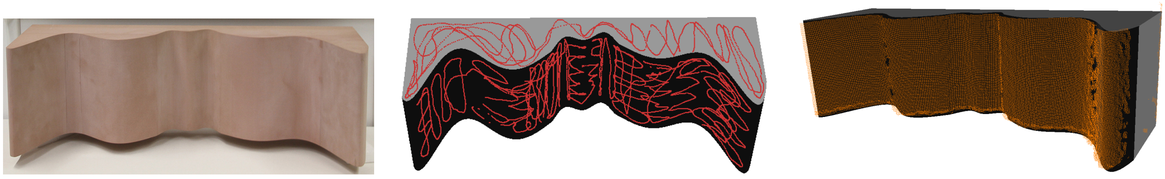

(a) Real 3D calibration object.

(b) Virtual 3D model.

(c) Virtual 3D model.

Figure 3: 3D calibration object and 3D model of the calibration object, aligned with 3D measurements (red: acquired with the point tip of the measurement arm, orange: captured with the Kinect depth camera).

such that it has the same position and orientation as the real 3D calibration object. To align the virtual 3D model with the 3D calibration object, sparse 3D measurements on the surface of the real 3D calibration object are acquired with the point tip of the measurement arm. Figure 3(b) shows such 3D points, colored in red. These 3D points are used for the alignment of the virtual 3D model with the real calibration object. The 3D point cloud and the 3D model are aligned with the Iterative Closest Point algorithm (ICP)(Besl and McKay, 1992)(Rusinkiewicz and Levoy, 2001). We use a point-to-triangle ICP variant which iteratively reduces the distances between the 3D point cloud (measured on the surface of the real object) and the 3D triangle mesh of the virtual model. First, the 3D point cloud and the 3D model are coarsely aligned manually. Then, the alignment is optimized with the ICP algorithm. In each iteration, the closest point on the triangle mesh is searched for each measured 3D point. Then, singular value decomposition is used to estimate a rotation and a translation which transforms the virtual 3D model, such that the average distance between both point sets is minimized. This iterative alignment reduces the average distance between the 3D points (consisting of 80.000 measurements) and the 3D model shown in Figure 3 to 0.2mm.

Camera Pose Estimation by Geometric Alignment. The geometric alignment between a 3D point cloud and a 3D model is computationally expensive. Therefore, as a preparational step, we create an octree that hierarchically divides the space around the 3D model into rectangular regions. This speeds up the detection of closest points on the surface of the 3D model. Only those triangles need to be inspected which are located in the same region of the hierarchical bounding volume as the 3D point measured with the depth camera. For each captured depth image, the pose T3 of the depth camera is estimated with geometric alignment using the ICP algorithm.

The ICP algorithm requires a coarse initial estimation of the depth camera's pose. To get such an initial estimation, we apply the hand-eye transformation calculated with the image based approach on the pose T1 of the measurement arm. An equally feasible approach would be to set the approximate camera pose for the first frame manually. Then, the hand-eye calibration calculated geometrically from previous frames can be used to initialize the camera poses of all other frames. Given the approximate pose of the depth camera, the following steps are repeated iteratively to improve the camera pose estimation with geometric alignment:

1. Render the 3D model with the current estimate of the camera parameters and use the rendered image as a validity filter. Reject all 3D measurements captured at pixels to which the 3D model does not get projected. This removes 3D measurements which do not belong to the surface of the calibration object.
2. Use the depth camera's pose estimation (R,t) with the following equation to transform each 3D measurements acquired with the depth camera from the camera coordinate system (p_{ccs}) to the world coordinate system (p_{wcs}):
$$p_{\text{wcs}} = R^{-1}(p_{\text{ccs}} - t) \tag{3}$$
3. For each 3D measurement: Find the closest point on the triangle mesh (the octree speeds up this calculation).
4. Trim the found point pairs to remove outliers: reject those 5% of the found point pairs, which have the largest distance between the measured and the found 3D point.
5. Calculate the transformation that minimizes the distance between both point sets with singular value decomposition.
6. Update the estimated camera pose by applying the calculated transformation on the previously estimated camera pose.

Figure 3(c) shows 3D measurements captured with a Kinect depth camera, geometrically aligned to the virtual 3D model of the calibration object.

4 ERROR METRICS

The quantitative evaluation of the hand-eye calibrations is subject to two major challenges:

1. The searched (”correct”) hand-eye transformation is not known and cannot be measured directly.
2. The ”correct” hand-eye transformation might be different for 3D measurements than for the 2D images captured with a depth camera. For example, the manual of the SwissRanger 4000 depth camera explicitly states that the 3D measurement’s coordinate system is not located at the optical center of the depth camera (MesaImaging, 2009).

As no ground truth data is available for the hand-eye calibration, the accuracy of the hand-eye calibration needs to be evaluated indirectly (without comparing the estimated hand-eye calibration to ”correct” reference values of the calibration). Furthermore, for applications which use both the 3D measurements and the 2D images acquired by a depth camera, the accuracy of the hand-eye calibration can not be assessed either with a 2D or with a 3D data based error metric alone. For these reasons, we use both a 2D and a 3D data based metric to evaluate the accuracy of the depth camera based hand-eye calibrations. Visualizations of both error metrics are shown in Figure 4.

2D Error Metric. We propose to use the ”normalized reprojection error” as 2D error metric. The unnormalized reprojection error measures the distance between the projection m of a 3D point M_{wcs} to the 2D image and the detected position of this point in the 2D image (m'). Here, M_{wcs} is the 3D position of a corner point of the 2D calibration pattern, measured with the point tip of the measurement arm as described in Section 2. For each frame of the evaluation sequence, the pose (R,t) of the depth camera is calculated from the pose of the measurement arm and the estimated hand-eye transformation with equation (1). Then, given the intrinsic camera calibration matrix K, the projection m of M_{wcs} onto the 2D image is calculated with

$$m = K[R|t]M_{\text{wcs}}. \tag{4}$$

The reprojection error increases when the camera is moved closer to the 2D calibration pattern. Thus, we normalize the projection error by the length of the 2D calibration pattern, to get the normalized reprojection error as a percentage of the calibration pattern’s size. Given the projections m_i and m_{i+1} of two adjacent corner points of the calibration pattern, the normalized reprojection error (m_i, m_i') is:

$$\text{NReprojErr}(m_i, m_i') = 100 \cdot \frac{\|m_i - m_i'\|_2}{\|m_i - m_{i+1}\|_2}. \tag{5}$$

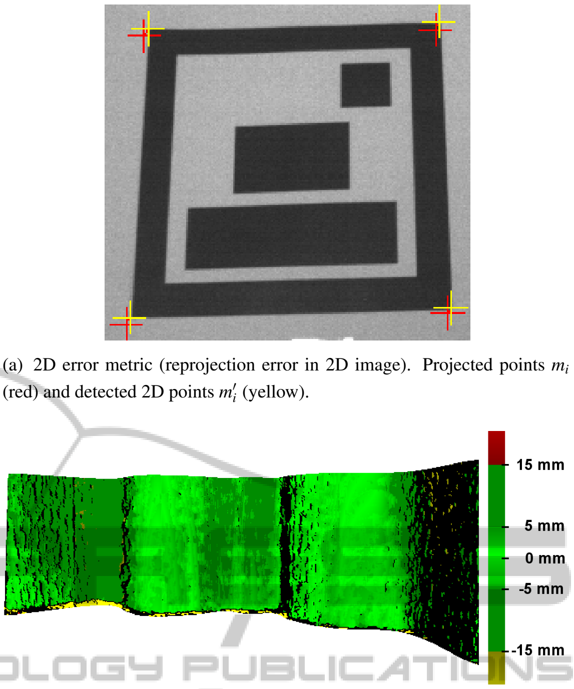
(a) 2D error metric (reprojection error in 2D image). Projected points m_i (red) and detected 2D points m_i' (yellow).

(b) 3D error metric: pixelwise difference between measured and real distance to the 3D calibration pattern.

Figure 4: 2D and 3D error metrics.

3D Error Metric. As 3D error metric, we use the distance between the 3D measurements of the depth camera and the surface of the calibration object. As described in Section 3, the 3D model used in this work was aligned with the real calibration project with an accuracy of 0.2mm. Thus, the 3D model provides ground truth data for the evaluation of the 3D measurements. To compare the depth measurements with this ground truth data, the camera pose is first calculated from the pose of the measurement arm and the estimated hand-eye calibration. Next, the 3D model is rendered from the current pose estimation of the depth camera. Then, the depth buffer values are compared with the depth values measured by the depth camera.

Please note, that even for a perfect hand-eye calibration, there are still 3D differences between the measured and the ground truth distance values. Such 3D differences are for example caused by measurement inaccuracies and systematic measurement errors of the depth camera. However, the total 3D error (caused both by inaccuracies in the hand-eye calibration and by other error sources) increases when the hand-eye calibration is inaccurate and decreases for accurate hand-eye calibrations. By using the same evaluation sequence for both proposed hand-eye calibration approaches, we are able to directly compare the accuracy of both hand-eye calibrations.

5 QUANTITATIVE EVALUATION

We evaluated the hand-eye calibrations with a structured light depth camera (Kinect) and with a time-of-flight depth camera (SwissRanger 4000). The Kinect calculates distances by projecting an infrared pattern on the captured scene and by analyzing the distortions of the projected pattern. It outputs 640 × 480 depth values. In contrast, the SwissRanger emits infrared light and measures the time it takes for the emitted light to return to the camera after it has been reprojected by the captured scene. The SwissRanger 4000 provides 176 × 144 depth measurements.

Evaluation Sequences. The calibration and evaluation sequences were captured hand-held, by moving the measurement arm with the rigidly coupled depth camera around the calibration objects. The 3D sequences were recorded such that most of the front shape of the calibration pattern was captured: for frames in which only a small part of the 3D calibration surface is visible, an unambiguous alignment of the 3D measurements with the 3D shape of the calibration object can not be calculated. Furthermore, both for the 2D and the 3D calibration sequences, more images were captured such that the calibration object covered a rather large part of the image: both image based pose estimations as well as 3D depth measurements become less accurate with increased distances. The 2D calibration was detected in 3410 images of the Kinect infrared camera and in 5111 images captured with the SwissRanger 4000. For the geometric hand-eye calibration, 809 Kinect depth images and 2866 SwissRanger depth images were used.

5.1 Accuracy

The results of the hand-eye calibrations are shown in Table 1 (Kinect) and in Table 2 (SwissRanger 4000). The SwissRanger captures less 3D measurements than the Kinect and the 2D image is more blurred and has a lower resolution. Therefore, the estimated camera poses vary more and the standard deviation is higher for the SwissRanger than for the Kinect depth camera.

Table 3 shows the accuracy as evaluated with the 2D evaluation metric (the reprojection error, see Section 4). Furthermore, Table 4 provides the results of the 3D evaluation metric. As noted in Section 4, the overall accuracy depends not only on the accuracy of the hand-eye calibration, but also on other factors such as the measurement accuracy of the depth camera. As the latter depends strongly on the distance between the camera and the captured object surfaces, the overall accuracy is specified for different ranges of measurement distances.

None of the two approaches (image based calibration and geometric calibration) is clearly more accurate than the other one. With the 2D evaluation metric, the image based calibration procedure performs better than the geometric hand-eye calibration (see Table 3). However, with the 3D evaluation metric, the geometric hand-eye calibration procedure performs better than the image based approach (Table 4). As explained in Section 4, the origin of a depth camera's 3D coordinate system is not necessarily at the optical center of the camera. Therefore, in view of the accuracy of the hand-eye calibration for the 3D measurements, the 3D evaluation metric is more conclusive than the 2D evaluation metric. Thus, the 3D measurement based hand-eye calibration seems to provide a more accurate hand-eye calibration for the 3D measurements.

Distances in the Calibration Sequences For most measurement distances, the geometric hand-eye calibration provides more accurate results in view of the 3D measurements than the image based calibration (see Table 4). However, for very close distances, the accuracy is lower than with the calibration of the image based approach. This effect is probably caused by the distribution of the distances in the sequences used for the hand-eye calibrations. Figure 5 shows the calibration sequences' distance distributions of the camera centers to the 2D and the 3D calibration pattern. The accuracy is best for those distances with most input data. Due to the prerequisites in view of the visibility and the size of the calibration objects in the images, the 2D images were captured a bit closer to the calibration object than the data of the 3D calibration sequences. This effect is stronger for the Kinect data because the Kinect cannot measure depth values for surfaces too close to the camera. In order to acquire depth measurements of the whole 3D calibration object (without missing surface parts), most Kinect depth images were recorded with a distance of about 1m. Thus, for the Kinect, the 3D data based hand-eye calibration is most accurate for those distances at which the Kinect is best operated (at 1m distance, the Kinect does not suffer from missing surface measurements and acquires more precise depth measurements than for larger distances).

Systematic Depth Measurement Errors. Depth cameras suffer from systematic depth measurement errors. This effect is shown by Figure 6 and is stronger for time-of-flight depth cameras than for the Kinect structured light depth camera. However, these

Table 1: Kinect: estimated hand-eye transformations (R,t) and standard deviations for Kinect depth camera. The rotation R is represented by a normalized axis angle, in degrees. The translation t is in mm.

Kinect	**Image based calibration**		**Geometric calibration**	
	median	**std**	**median**	**std**
R	(-0.28, 0.80, 93.07)	(0.82, 0.73, 0.22)	(0.10, -0.27, -93.03)	(0.71, 0.57, 0.47)
t	(13.30, -54.42, 80.48)	(13.08, 10.10, 7.20)	(22.07, -58.04, 93.23)	(13.22, 5.76, 8.14)

Table 2: SwissRanger 4000: estimated hand-eye transformations (R,t) and standard deviations for SwissRanger depth camera. The rotation R is represented by a normalized axis angle, in degrees. The translation t is in mm.

SR4000	**Image based calibration**		**Geometric calibration**	
	median	**std**	**median**	**std**
R	(1.36, 0.14, 89.87)	(7.04, 6.80, 2.03)	(0.17, 1.63, 90.10)	(1.23, 1.29, 1.08)
t	(-11.63, 69.38, 103.68)	(18.27, 10.23, 13.00)	(-12.50, 40.80, 113.56)	(15.93, 31.26, 6.02)

Table 3: **2D error metric:** Median of normalized reprojection errors. All values are in percent (ratio of reprojection error to the size of the 2D calibration pattern in the 2D image).

Distance depth camera - surface	**Kinect: image based calibration**	**Kinect: geometric calibration**	**SR4000: image based calibration**	**SR4000: geometric calibration**
450-599	1.53	2.95	7.54	10.26
600-749	1.75	2.85	5.59	7.60
750-899	2.08	3.91	4.21	5.37
900-1049	2.34	5.13	3.44	4.08
1050-1199	2.75	6.55	3.29	4.62
1200-1349	2.86	7.77	3.67	5.67
1350-1499	2.96	9.14	4.79	7.21
1500-1649	3.20	10.56	6.21	8.87

Table 4: **3D error metric:** Median difference between the 3D measurements and the ground truth (3D position on the 3D model of the calibration object). All values are in mm.

Distance depth camera - surface	**Kinect: image based calibration**	**Kinect: geometric calibration**	**SR4000: image based calibration**	**SR4000: geometric calibration**
450-599	3.70	13.01	8.90	19.05
600-749	4.88	12.35	10.17	16.81
750-899	6.87	4.84	11.42	12.58
900-1049	10.84	4.04	10.89	8.60
1050-1199	18.97	8.18	10.63	8.24
1200-1349	26.24	11.61	10.81	9.69
1350-1499	38.26	23.32	7.74	8.41
1500-1649	50.58	35.97	10.83	9.41

systematic errors do not seem to have a strong effect on the accuracy of the hand-eye calibration, as the 3D data based hand-eye calibration also provides good results for the SwissRanger time-of-flight depth camera. This might be due to the symmetry of the systematic measurement errors, which might lessen systematic effects when aligning the 3D measurements with the 3D model of the calibration object.

Combined 2D and 3D Calibration. To evaluate whether the accuracy of the hand-eye calibration could be improved by combining the image based and the 3D data based approach, we attached three markers on the wall above the 3D calibration object. The size of the markers was chosen such that they were fully visible when recording a sequence of the 3D calibration pattern. Then, for each frame, we calculated the hand-eye calibration both with the 2D images and

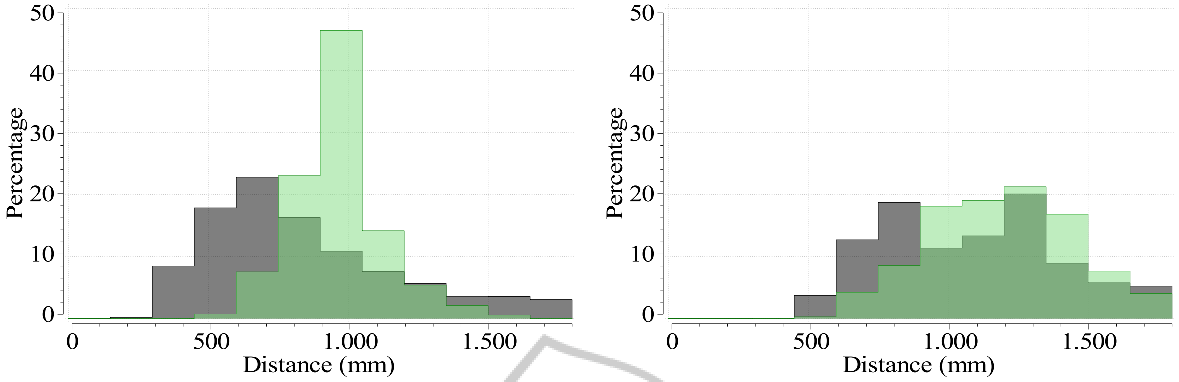

(a) Kinect hand-eye calibration.

(b) SR4000 hand-eye calibration.

Figure 5: Distribution of the distances from the camera centers to the calibration objects in the calibration sequences. Grey: image based, green: geometric.

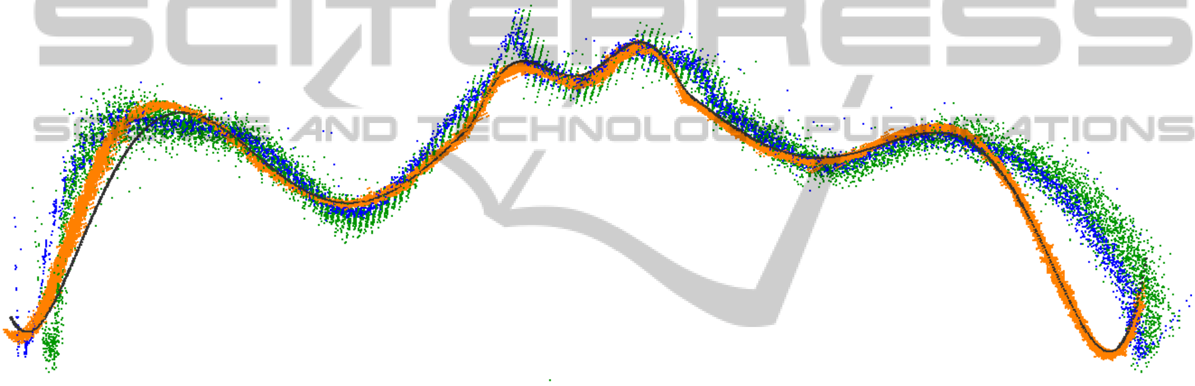

Figure 6: Curvature of calibration object (black) and aligned 3D point clouds measured by different depth cameras (orange: Kinect, blue: SwissRanger4000, green: CamCube 3.0). Note the systematic differences of the shape of the real object and the measured shapes.

with the 3D data. However, this combined approach neither increased the accuracy of the image based nor the accuracy of the 3D data based calibrations. The three markers covered only a rather small area of the image when both the markers and the 3D calibration pattern were visible in the same camera image, which decreased the accuracy of the image based camera pose estimations. Thus, the estimated camera poses were too inaccurate to improve the results.

5.2 Processing Time

The hand-eye calibrations were calculated with a 3.07 Ghz processor, using a single-core CPU implementation. For the Kinect, the estimation of the image based pose estimations used for the hand-eye calibration took 18 milliseconds per frame. The 3D data based camera pose estimations took 167 seconds per frame. For the SwissRanger 4000, the camera pose estimation times were 7 milliseconds per frame (image based), respectively 47 seconds per frame (3D data based).

6 CONCLUSIONS

For depth cameras, the hand-eye transformation between the camera and a measurement arm can either be estimated using 2D images or the 3D measurements captured by the depth camera. We have introduced two hand-eye calibration algorithms which differ only in the way the camera pose is estimated (either 2D or 3D data based) and which are thus directly comparable. These algorithms were evaluated quantitatively, both with a 2D and a 3D evaluation metric.

The quantitative evaluation shows that both methods provide accurate results. The 3D data based calibration provides more accurate results in view of the 3D measurements. However, this improved accuracy comes at the cost of the prerequisite of a 3D calibration object and its accurate 3D model. Further, the surface of the 3D model needs to be sampled with the point tip of the measurement arm in order to align the 3D model and the calibration object. Thus, the 3D data based approach requires a more labour intensive preparation than the image based approach (for which it is sufficient to print a marker and to measure the four 3D coordinates of its corner points with the measurement arm). Furthermore, the 3D data based hand-eye calibration is much more computationally expensive than the 2D image based approach. On a CPU, the computation time is about one day for the 3D data based approach when 500 Kinect depth images are used. With the image based approach, the hand-eye calibration can be calculated in a few seconds. Thus, the 3D data based approach is well suited for applications which require precise 3D data. In contrast, the image based approach is slightly less accurate.

In future work, we will investigate different shapes of the calibration objects. The 3D calibration object used in this paper has a non-varying shape along its vertical axis. During the evaluation, this turned out to pose difficulties for the geometric alignment of the 3D measurements with the 3D model: the alignment has a degree of freedom along the vertical axis of the 3D calibration object. Thus, the estimated alignment can slide along this axis. Therefore, future 3D calibration objects should preferably have a shape that also varies along the vertical axis. Further, it is possible to improve the accuracy of the image based hand-eye calibration by replacing the image marker with a more diversely textured object, such as a 2D poster. As the texture of a poster is known beforehand, it could be used to train sophisticated feature detection algorithms (Lepetit and Fua, 2006). Such an algorithm could further enhance the accuracy of the image based camera pose estimation and thus the accuracy of the image based hand-eye calibration.

ACKNOWLEDGEMENTS

This work was partially funded by the German Research Foundation (DFG) within the GRK 1362 (http://www.gkmm.tu-darmstadt.de).

REFERENCES

Besl, P. and McKay, N. (1992). A method for registration of 3-d shapes. In *IEEE Trans. on Pattern Analysis and Machine Intell.*, volume 14(2), pages 239–256.

Fuchs, S. (2012). *Calibration and Multipath Mitigation for Increased Accuracy of Time-of-Flight Camera Measurements in Robotic Applications*. PhD thesis, TU Berlin, Germany.

Kahn, S., Bockholt, U., Kuijper, A., and Fellner, D. W. (2013). Towards precise real-time 3d difference detection for industrial applications. *Computers in Industry*, pages 1–14.

Kahn, S. and Kuijper, A. (2012). Fusing real-time depth imaging with high precision pose estimation by a measurement arm. In *2012 International Conference on Cyberworlds (CW)*, pages 256–260.

Kim, D.-W. and Ha, J.-E. (2013). Hand/eye calibration using 3d-3d correspondences. *Applied Mechanics and Materials*, 319:532–535.

Lepetit, V. and Fua, P. (2006). Keypoint recognition using randomized trees. *Pattern Analysis and Machine Intelligence, IEEE Transactions on*, 28(9):1465–1479.

MesaImaging (2009). SR4000 user manual (version 2.0).

Piatti, D. (2011). *Time-of-Flight cameras: tests, calibration and multi-frame registration for automatic 3D object reconstruction*. PhD thesis, Politecnico di Torino, Italy.

Reinbacher, C., Ruther, M., and Bischof, H. (2012). Ronect: Hand mounted depth sensing using a commodity gaming sensor. In *21st International Conference on Pattern Recognition (ICPR)*, pages 461–464.

Rusinkiewicz, S. and Levoy, M. (2001). Efficient variants of the ICP algorithm. *In Proc. 3rd Intl. Conf. on 3-D Digital Imaging and Modeling*, pages 224–231.

Stoyanov, T., Mojtahedzadeh, R., Andreasson, H., and Lilienthal, A. J. (2012). Comparative evaluation of range sensor accuracy for indoor mobile robotics and automated logistics applications. *Robotics and Autonomous Systems*. Online first 10/2012.

Strobl, K. H. and Hirzinger, G. (2006). Optimal hand-eye calibration. In *Proc. of the IEEE/RSJ Int. Conf. on Intelligent Robots and Systems*, pages 4647–4653.

Tsai, R. Y. and Lenz, R. K. (1988). A new technique for fully autonomous and efficient 3d robotics hand-eye calibration. In *Proc. of the 4th international symposium on Robotics Research 1998*, pages 287–297.

Willert, V., Haumann, D., and Hartkopf, S. (2012). Methode zur Hand-Auge-Kalibrierung von 3D-Kameras. EP12190676.2.